An investigation of composition, morphology, mechanical properties, and microdamage accumulation of human type 2 diabetic bone

Marissa Britton, Genna E Monahan, Colin G Murphy, Stephen R Kearns, Aiden T Devitt, Anaïs Okwieka, Stéphane Jaisson, Laurence van Gulick, Abdelilah Beljebbar, Halima Kerdjoudj, et al.

Bone 187 (2024) 117190

Contents lists available at ScienceDirect

Bone

journal homepage: www.elsevier.com/locate/bone

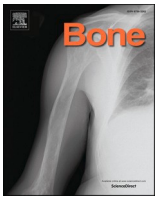

Full Length Article

An investigation of composition, morphology, mechanical properties, and microdamage accumulation of human type 2 diabetic bone

Marissa Britton [a], Genna E. Monahan [a], Colin G. Murphy [b], Stephen R. Kearns [b], Aiden T. Devitt [b], Anaïs Okwieka [c], Stéphane Jaisson [c], Laurence Van Gulick [d], Abdelilah Beljebbar [d], Halima Kerdjoudj [e], Jessica Schiavi [f], Ted J. Vaughan [a,*]

[a] Biomechanics Research Centre (BioMEC), Biomedical Engineering, College of Science and Engineering, University of Galway, Galway, Ireland
[b] Department of Orthopaedics, Galway University Hospitals, Galway, Ireland
[c] University of Reims Champagne-Ardenne, CNRS, Extracellular Matrix and Cell Dynamics Unit (MEDyC) UMR, Reims, France
[d] Université de Reims Champagne-Ardenne, BioSpecT Unit, EA 7506 Reims, France
[e] Biomatériaux et Inflammation en Site Osseux (BIOS), Université de Reims Champagne Ardenne, EA 4691 Reims, France
[f] University of Lorraine, CNRS, LRGP, F-54000 Nancy, France

ARTICLE INFO

Keywords:
Bone fragility
Trabecular bone mechanics
Type-2 diabetes

ABSTRACT

This study investigates the biomechanics of type 2 diabetic bone fragility through a multiscale experimental strategy that considers structural, mechanical, and compositional components of ex vivo human trabecular and cortical bone. Human tissue samples were obtained from the femoral heads of patients undergoing total hip replacement. Mechanical testing was carried out on isolated trabecular cores using monotonic and cyclic compression loading and nanoindentation experiments, with bone microdamage analysed using micro-computed tomography (CT) imaging. Bone composition was evaluated using Raman spectroscopy, high-performance liquid chromatography, and fluorometric spectroscopy. It was found that human type 2 diabetic bone had altered mechanical, compositional, and morphological properties compared to non-type 2 diabetic bone. High-resolution micro-CT imaging showed that cores taken from the central trabecular region of the femoral head had higher bone mineral density (BMD), bone volume, trabecular thickness, and reduced trabecular separation. Type 2 diabetic bone also had enhanced macro-mechanical compressive properties under mechanical loading compared to non-diabetic controls, with significantly higher apparent modulus, yield stress, and pre-yield toughness evident, even when properties were normalised against the bone volume. Using nanoindentation, there were no significant differences in the tissue-level mechanical properties of cortical or trabecular bone in type 2 diabetic samples compared to controls. Through compositional analysis, higher levels of furosine were found in type 2 diabetic trabecular bone, and an increase in both furosine and carboxymethyl-lysine (an advanced glycation end-product) was found in cortical bone. Raman spectroscopy showed that type 2 diabetic bone had a higher mineral-to-matrix ratio, carbonate substitution, and reduced crystallinity compared to the controls. Together, this study shows that type 2 diabetes leads to distinct changes in both organic and mineral phases of the bone tissue matrix, but these changes did not coincide with any reduction in the micro- or macro-mechanical properties of the tissue under monotonic or cyclic loading.

1. Introduction

Type 2 diabetic patients have up to a 3-fold increase in bone fracture risk [1–7] when compared to non-type 2 diabetic patients. However, there are clinical challenges associated with predicting fracture risk in this cohort as measures of bone mineral density (BMD) tend to be normal, or even higher than non-diabetic controls [8]. This implies that type 2 diabetes (T2D) impairs the quality of the bone matrix itself, whereby the intrinsic properties of bone tissue matrix are deteriorated. Yet, the precise factors that contribute to sub-tissue alterations in the bone matrix and their effect on whole-bone fragility remain poorly understood.

* Corresponding author at: Biomechanics Research Centre (BMEC), School of Engineering, College of Science and Engineering, University of Galway, Galway, Ireland.
E-mail address: ted.vaughan@universityofgalway.ie (T.J. Vaughan).

https://doi.org/10.1016/j.bone.2024.117190
Received 13 March 2024; Received in revised form 7 June 2024; Accepted 30 June 2024
Available online 2 July 2024

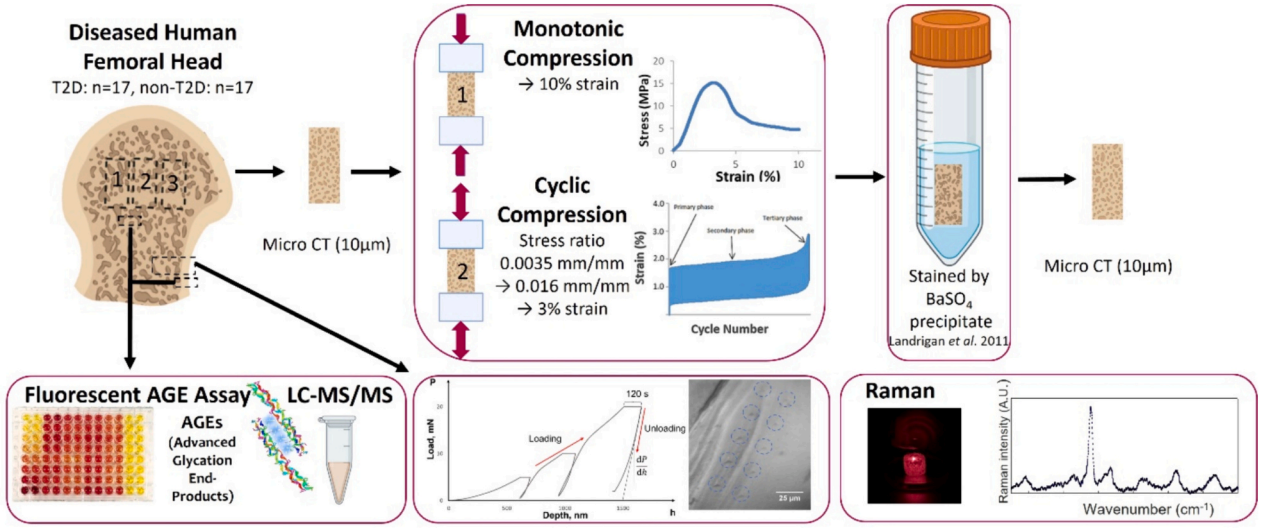

Fig. 1. Study design showing bone cores removed from the femoral head, and the characterisation methods used to evaluate the bone cores morphologically, mechanically, and compositionally.

It is thought that the hyperglycaemic state in T2D impairs tissue properties by forming non-enzymatic cross-links and adducts known as advanced glycation end products (AGEs) in the collagenous proteins of the bone matrix. The accumulation of AGEs is known to lead to a disruption of bone homeostasis [9] and affect the bone cells, leading to decreased osteoblast activity [10,11], decreased osteoblast attachment to the collagen matrix [12], and decreased osteoclastogenesis [13]. Consequently, these alterations have repercussions on the mineral and collagen components of bone with lower levels, of bone formation and resorption markers found in T2D leading to the implication that bone turnover in T2D is lower [14,15]. Furthermore, the presence of AGEs causes a decline in the solubility of collagen [13]. The mineralisation of the tissue is also affected due to T2D with hyperglycaemia disrupting the mineralisation phase of osteoblasts [16]. Additionally, the mineralisation quality is thought to possibly be altered due to secondary mineralisation not developing as it should [17].

The accumulation of AGEs in the bone matrix is thought to lead to more brittle behaviour. Despite this common assertion [18–20], there is a lack of experimental data that quantitatively demonstrates any mechanistic relationship between AGE accumulation and mechanical properties in human type 2 diabetic bone [21]. Much of the current understanding of the mechanics of bone fragility in T2D has been generated using in vitro models [22–27], whereby animal or human tissue has been immersed in a ribose solution to promote non-enzymatic glycation of the protein network. However, previously we demonstrated that in vitro glycation models are severely limited by the fact that they induce AGE levels that are much higher than what occurs physiologically [28]. In contrast, many human studies [29,30] have reported no significant differences in fluorescent AGEs in the femoral neck and head of T2D trabecular bone tissue compared to non-diabetic controls. Only a limited number of human studies have actually reported elevations in either bulk fluorescent AGEs [31] or pentosidine [29] in trabecular bone tissue from the femoral head and neck, respectively. It should be noted that the Sihota et al. [31] study involved patients who had experienced their first fragility fracture, whereas other studies involved patients with osteoarthritis, which may explain the increased levels of AGEs found in the bulk fluorescent measurement by Sihota et al. [31] as osteoporosis is also associated with an increase in levels of AGEs [32]. Furthermore, there is a poor understanding of the relationship between AGE accumulation and bone tissue mechanics in T2D due to the complicated hierarchical structural organisation of bone tissue and the related damage accumulation process. Uniaxial compression testing of trabecular cores from femoral heads has revealed no discernible differences in the mechanical properties of human type 2 diabetic bone [30,33], compared to non-diabetic controls, with Hunt et al. [29] showing that male type 2 diabetic bone had higher Young's modulus, yield stress, and ultimate stress in femoral neck trabecular cores than non-diabetic controls [29]. Only one study [31] has found impaired mechanical properties in diabetic trabecular bone. Additionally, one study [30] observed an increase in indentation distance in diabetic cortical bone using reference point indentation testing. Still, the mechanical properties were not correlated to AGE accumulation in this study. These are the only results in the literature that have shown impaired tissue-level properties in T2D. This highlights that, rather than AGE accumulation, other mechanisms must be responsible for fragility in T2D. These mechanisms are yet to be elucidated.

During their lifetime, bones are subjected to repeated cyclic loading that leads to the accumulation of microdamage in the tissue. Microdamage is thought to be a biomechanically significant component of bone quality [34], which more frequently develops in vivo in older people [35–38]. Microdamage is generally repaired through the process of bone remodelling. Osteoblast and osteoclast cells actively maintain a healthy bone tissue matrix [39–41]. However, the onset of T2D leads to complex pathophysiological changes that ultimately disrupt normal bone homeostasis [9] and alters the bone remodelling process [14,15]. The altered remodelling process in T2D has been hypothesised to lead to an increase in microdamage accumulation in bone [42], possibly leading to impaired properties. However, there have been limited experimental investigations on the accumulation of microdamage in diabetic bone. While Tang and Vashishth [43] showed using an in vitro glycation model of human bone that higher levels of microdamage accumulated in glycated samples compared to control bones, only one study has characterised microdamage in actual type 2 diabetic tissue, to date. Here, Sacher et al. [42] used uniaxial compression testing to show that, while there was an altered distribution of microdamage in type 2 diabetic bone, there was no difference in the total accumulation of microdamage compared to non-diabetic controls following uniaxial compression. However, this study used monotonic loading, which does not replicate the repeated cyclic loading that bone experiences in vivo due to daily activities. Many early studies on non-diabetic bone [44–46] have used cyclic loading to establish relationships between the proportion of fatigue life, mechanical properties, and microdamage accumulation. In particular, Lambers et al. (2013) showed that even small amounts of microdamage accumulation in human vertebral cancellous bone following cyclic loading may have substantial effects on biomechanical performance. Such mechanisms could play a role in diabetic bone

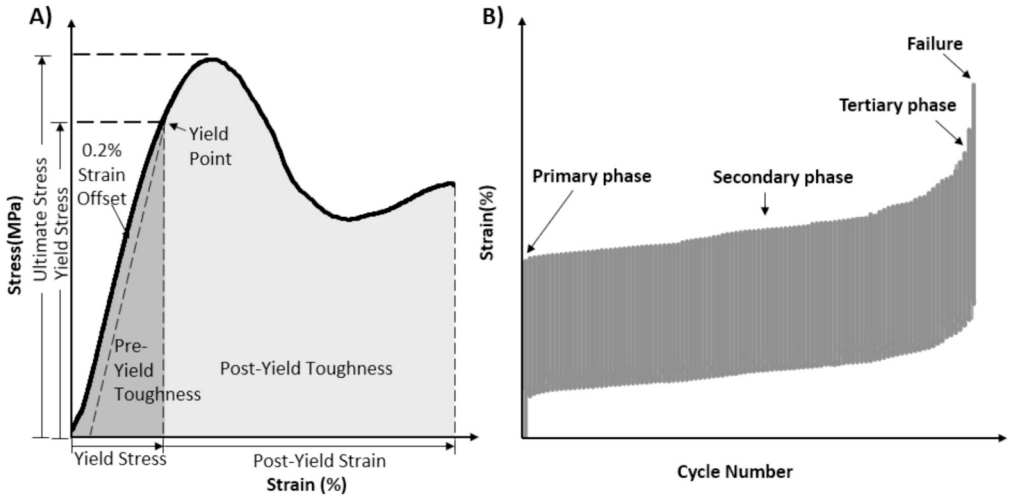

Fig. 2. A) Stress-strain curve schematic of monotonic compression to 10 % strain applied to the core one cohort, B) strain versus cycle number schematic of cyclic compression to 3 % strain applied to the core two cohort.

fragility, however, the relationship between microdamage accumulation and the biomechanical performance of human type 2 diabetic bone has not yet been investigated.

The objective of this study is to investigate the roles of bone composition and microdamage accumulation on the mechanical properties of type 2 diabetic femoral head trabecular bone tissue under both monotonic and cyclic loading. Cylindrical cores from human femoral heads were extracted and mechanically tested using monotonic, cyclic compression, and nanoindentation testing. Morphological analysis was conducted using micro-computed tomography (micro-CT) imaging, while microdamage accumulation was quantified through barium sulfate staining. The collagen content, AGE concentration, and mineralisation of the bone were compositionally analysed using fluorometric analysis, LC-MS/MS, and Raman spectroscopy.

2. Materials and methods

2.1. Bone samples

Fig. 1 shows a schematic that describes the study design. Femoral heads were obtained from age and sex-matched patients, with T2D (74 ± 9 years) and without T2D (74 ± 9 years). These patients underwent total hip replacement for clinically diagnosed osteoarthritis (OA) and osteoporosis (OP) at two Galway hospital sites, Merlin Park University Hospital and University Hospital Galway. All research procedures were approved by the Clinical Research Ethics Committee, Galway University Hospitals, Galway, Ireland. The research was performed following the relevant guidelines and regulations of the University of Galway. The groups were categorised as follows; T2D ($n = 17$) and non-T2D ($n = 17$). None of the patients examined had any recorded comorbidities apart from osteoarthritis or osteoporosis, nor were they on medications known to affect bone metabolism (e.g. glucocorticoids, antiretroviral medications, bisphosphonates, teriparatide, or denosumab). HbA_{1c} levels for $n = 10$ of the type 2 diabetic group were collected prior to surgery (57.6 ± 14.2 mmol/mol or 7.4 ± 1.3 %), and the HbA_{1c} for the remaining type 2 diabetic and non-type 2 diabetic samples were unavailable. Three cylindrical cores of trabecular bone were removed from the femoral head, along the main trabecular direction, with one of these cores undergoing monotonic compression, another undergoing cyclic compression, and the third core being used as a control. Microdamage was measured by staining the samples with barium sulfate and using micro-CT imaging to measure the accumulation of damage. Sections from the femoral head were also tested using nanoindentation to measure tissue-level mechanical properties. Compositional analysis using fluorometric assays, LC-MS/MS, and Raman spectroscopy was carried out on both trabecular and cortical tissue to measure the accumulation of AGEs.

2.1.1. Sample preparation

Upon removal from the patient, femoral heads were wrapped in PBS-soaked gauze and stored in a sterile container. Samples were then frozen at −20 °C before processing. Samples were defrosted and scanned using a micro-CT scanner (μCT100, Scanco Medical AG, Bassersdorf, Switzerland) (see Section 2.1.2). The bone was then cut in a plane orthogonal to the main trabecular direction (MTD), using a low-speed saw (ISOMET™ Low Speed Saw, Buehler, IL, USA) under constant water irrigation. A second cut parallel to the first cut was performed to obtain a ~21 mm thick bone slice. Fig. 1 shows a schematic of the three cylindrical samples that were extracted from the central trabecular region of the femoral head using a diamond-tipped coring tool with an inner diameter of 8 mm. Bone marrow was removed from the sample using a water jet while the sample was underwater to reduce any additional microdamage. The cores were then scanned at a 10 μm resolution to measure the morphological properties. The samples to undergo mechanical testing were glued using cyanoacrylate (Prism 401, Loctite, Newington, CT, USA) into brass endcaps, to limit end-artefacts and allowed to cure at 4 °C overnight while the sample remained wrapped in PBS-soaked gauze.

2.1.2. Micro CT scanning

Micro-CT images of the full femoral heads were obtained at a voxel size of 36.8 × 36.8 × 36.8 μm^3 using a high-resolution micro-CT scanner (μCT100, Scanco Medical AG, Bassersdorf, Switzerland) with settings of 70 kVp, 114 mA and 300 ms [47]. Samples were placed in a sample holder to allow for the anatomical positions to be aligned with the axis of the micro-CT machine. The sample holder was then filled with PBS to cover the femoral head. The bone morphology evaluation script was used to determine the main trabecular direction (MTD). Cores one and two from each of the femoral heads were also scanned at 10 μm resolution to determine the morphological properties: bone volume fraction (BV/TV), connectivity density (Conn.D, $1/mm^3$), bone mineral density (mg HA/cm^3), tissue mineral density (mg HA/cm^3), trabecular number (Tb.N, 1/mm), trabecular thickness (Tb.Th, mm) and trabecular separation (Tb.Sp, mm). Bone mineral density is the mean attenuation value of the volume of interest including marrow spaces, and tissue mineral density measures only the mean attenuation value of the segmented region or the bone tissue only. Images were segmented using a threshold of 617 mg HA/cm^3 and a Gaussian filter of sigma 1.2 and support 2 was used on the raw images to remove noise.

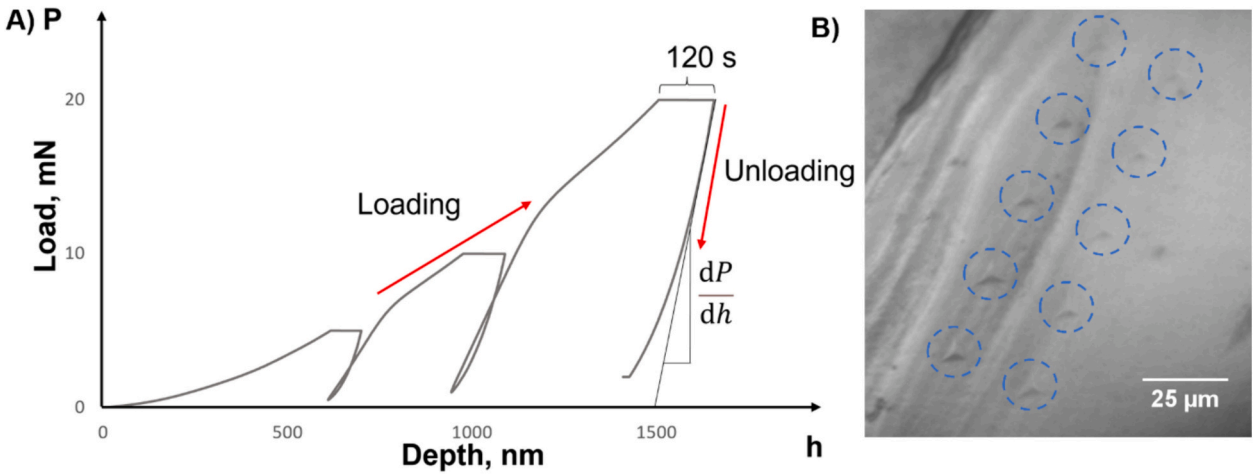

Fig. 3. (A) Schematic for nanoindentation loading profile. (B) Embedded trabecular bone that shows indented regions.

2.1.3. Mechanical analysis

2.1.3.1. Uniaxial monotonic compression. All monotonic mechanical testing was carried out on a uniaxial testing machine (Zwick/Roell, Ulm, Germany) with a 2.5 kN load cell. The cores were wrapped in PBS-soaked gauze to maintain hydration during the test and all tests were carried out at a strain rate of 0.5 % s^{-1}. Ten preconditioning cycles between 0 and 0.3 % strain were carried out as is standard in the literature [48]. Core one from each femoral head underwent monotonic compression until a strain of 10 %. A schematic of the monotonic compression stress-strain curve is shown in Fig. 2A. The apparent modulus was determined from the linear best fit to the steepest 0.2 % of the linear portion of the curve. The yield point was determined using the 0.2 % offset method. The pre-yield toughness was evaluated as the total area under the curve before the yield point and the toughness was calculated as the total area under the curve. The post-yield toughness was evaluated as the total area under the curve after the yield point.

2.1.3.2. Cyclic compression. All cyclic mechanical testing was carried out on a uniaxial testing machine (Zwick/Roell, Ulm, Germany) with a 2.5 kN load cell. The cores were wrapped in PBS-soaked gauze to maintain hydration during the test and all tests were carried out at a strain rate of 0.5 % s^{-1}. Ten preconditioning cycles between 0 and 0.4 % strain were carried out. Core two from each femoral head underwent cyclic compression testing [46,49]. To ensure loading was beyond the initial toe region of the stress-strain curve, the applied forces were measured at a strain cycle of 0.0035 mm/mm to 0.016 mm/mm from the initial cycles across each sample. These forces were then applied to enable cyclic loading of each sample. These are equivalent to the normalised relationship σ/E_t where σ is the stress and E_t is the tangent modulus at the applied strains. The cyclic compression was carried out until a predefined failure threshold of 3 % strain was reached, which was chosen based on preliminary testing that was found to capture the three phases of cyclic behaviour. Fig. 2 illustrates these three phases where (i) in the primary phase, the strain accumulation per cycle falls, (ii) in the secondary phase, the strain accumulation per cycle is constant and (iii) in the tertiary phase, the strain accumulation per cycle increases. The initial apparent modulus was determined from the linear best fit to the steepest 0.2 % of the first loading cycle of the cyclic fatigue curve, while the final apparent modulus was determined from the steepest 0.2 % of the final loading cycle. Across the tests carried out, the mechanical properties that were evaluated will be the number of cycles to failure (N_f), initial apparent modulus ($E_{initial}$), final apparent modulus (E_{final}), the percentage reduction in modulus, and energy dissipation as the area of the cyclic loading curves.

2.1.3.3. Nanoindentation testing. The tissue-level material properties were determined using nanoindentation. The samples were dehydrated in a series of ascending ethanol baths to prepare for embedding, whereby the cores were embedded in an epoxy resin (EpoThin2™, Buehler, IL, USA) and placed under vacuum to allow the epoxy to fill all large porous spaces. Dehydration of the sample does influence the nanoindentation results by leading to a higher modulus and hardness of bone [50]. Silicon carbide paper was used to remove epoxy to expose the test surface, which was then polished using a series of descending diamond suspension pastes (9 µm, 3 µm, 1.5 µm, and 0.05 µm) with polishing cloths on a polishing machine (MetaServ® 250 Grinder-Polisher with Vector® LC Power Head, Buehler, IL, USA). Using an ultrasonic bath and deionized water, the samples were washed between each polishing phase. The nanoindentation was carried out on a Nano-Indenter G200 (Keysight Technologies, CA, USA) with a Berkovich diamond indenter tip, with calibration of the machine performed using fused silica. Ten indents were made on the trabecular bone and cortical interstitial bone of each sample, with all indents positioned at least 10 µm away from the edge of the sample and 15 µm from neighbouring indents within the array. Fig. 3 shows a schematic of the loading profile used, which consisted of two conditioning steps that reached loads of 25 % max load and 50 % max load, followed by a third step that reached the max load of 20 mN. A hold period of 120 s was included after each loading peak was reached, which together with the multiple loading cycles, reduced the effects of time-dependent plasticity [51–54]. Upon unloading, the rate of thermal expansion was measured by holding the indenter at 10 % of the max load for 120 s to calibrate the thermal drift correction factor ahead of further data analysis.

The data obtained from the indentation tests were analysed to determine the Young's modulus and hardness of the samples, assuming a Poisson's ratio of 0.3, using the in-built Oliver and Pharr method (Keysight NanoSuite Software).

2.1.3.4. Microdamage analysis. After core one and two had undergone monotonic and cyclic tests, the microdamage was quantified by barium sulfide staining and micro-CT analysis in both the type 2 diabetic and non-diabetic groups. From each femoral head, core three, which had not undergone any mechanical testing, was used as a control to measure the pre-existing microdamage. To quantify microdamage accumulation, the damaged specimens, and the control specimen were stained with a barium sulfate solution [55] by soaking in an aqueous solution of equal parts 0.5 M $BaCl_2$, acetone, and PBS for 72 h followed by 0.5 M $NaSO_4$, acetone, and PBS for 72 h, all under vacuum. Finally, the specimens were agitated in buffered saline solution to remove excess $BaSO_4$ precipitates for 1 h. All specimens were scanned at 10 µm resolution, 70 kVp voltage, and 114 µA current with 200 ms integration time. A Gaussian

filter of sigma 1 and support 2 was used on the raw images to remove noise [56]. Different thresholds were used to determine the volume of bone and the volume of $BaSO_4$. Voxels with intensities greater than native 9000, corresponding to 631.1 mg HA/cm^3, and less than native 23,500, corresponding to 1965.6 mg HA/cm^3, were taken to be bone and voxels with intensities greater than native 23,500 were taken to be $BaSO_4$.The damaged volume was defined as the volume of $BaSO_4$ divided by the total volume of bone.

2.1.4. Bone compositional analysis

2.1.4.1. Raman micro-spectroscopy and spectral analysis. Raman micro-spectroscopy was used to evaluate the compositional properties of type 2 diabetic, and non-diabetic bone tissue. The properties measured were the mineral-to-matrix ratio, carbonate substitution, crystallinity, matrix maturity, helical status, hydroxyproline-to-proline ratio, and amide I-to-amide III ratio. This work was carried out using a similar methodology to Van Gulick et al. [57]. A HE-785 Raman spectrometer (Jobin-Yvon-Horiba, Longjumeau, France) was used to record the Raman spectra. This system included a high efficiency (HE) spectrometer with a fixed 950 g/mm grating coupled to a matrix charge coupled device (CCD) detector that was cooled by the Peltier effect at 200 K (Andor Technologies, Belfast, Northern Ireland). The excitation source and the detecting system were connected with a fibre probe (InPhotonics, MA, USA). The probe head included a bandpass filter, a beam splitter, a lens, a mirror, and a long pass filter. The 5 mm-focal-distance fibre probe was mounted on a z-adjustable holder to ensure optimum acquisition repeatability and enhance focus on the sample. The excitation wavelength of the laser source for illumination was set at 785 nm and was provided by an OEM diode laser (Process Instruments Inc., UT, USA) This device offers high throughput, sensitivity, and wavelength stability even when the temperature fluctuates. Each spectrum was measured with a 10-s integration time, with 10 measurements made per sample. Data acquisition was performed using the Labspec 5.0 software (Jobin-Yvon-Horiba).

Raman data were processed using Matlab (Mathworks, MA, USA). The raw spectra required multiple data processing steps, which consisted of instrument response correction, wave number calibration, fluorescence background subtraction, cosmic ray removal, and baseline corrected using a fifth polynomial fit. The data was smoothed using a seven-point Savitzky-Golay technique. A Standard Normal Variate (SNV) technique was used to normalise the resultant spectra. The second derivative spectra were calculated and used to identify the frequencies of underlying sub-bands. From this analysis, A minimum in the second derivative of a spectrum corresponds to local frequencies of collagen bands in the original spectrum. The full width at half-maximum of these sub-bands was manually selected as the starting conditions. The curve fitting procedure was then applied using a mixed Gaussian and Lorentzian to estimate quantitatively the area of each Raman band intensities of collagen. Comparisons of the χ^2 values and the residuals of the fits were used as the criteria for assessing the quality of fit.

2.1.4.2. Liquid chromatography coupled to tandem mass spectrometry (LC-MS/MS). As the glycation reaction is a complex process involving early and late steps, two different glycation products have been quantified to evaluate each phase of the process. Firstly, furosine concentrations were evaluated to provide information about the formation of Amadori products during the early phase of glycation. Furosine is an analytical surrogate for the adduct Nε-1-deoxyfructosyl (FL) and is a by-product formed during acid hydrolysis of FL [58,59]. Secondly, Carboxymethyl Lysate (CML) was evaluated to provide information about the later phase of glycation that involved oxidative reactions (e.g. formation of AGEs).

All samples were subjected to acid hydrolysis with 6 M hydrochloric acid for 18 h at 110 °C. Hydrolysates were evaporated to dryness twice under a nitrogen stream. Furosine and CML were then quantified by liquid chromatography coupled to tandem mass spectrometry (LC-MS/MS). Briefly, dried hydrolysates were resuspended in 100 µl of 125 mM ammonium formate containing 1 µM of d_2-CML and 1 µM d_4-furosine, used as internal standards, and filtered using Uptidisc PTFE filters (4 mm, 0.45 µm, Interchim, France) prior to LC-MS/MS analysis.

Furosine quantification was performed using a LC20 chromatographic system (Shimadzu, Kyoto, Japan) equipped with a Kinetex XB-C18 column (100 × 3.0 mm, 2.6 µm – Phenomenex, CA, USA) with a gradient program composed of 5 mM ammonium formate (pH 2.9) as mobile phase A and 100 % acetonitrile as mobile phase B. The flow rate was constant at 0.3 ml/min during all separation steps. The gradient program was as follows: 0–0.1 min: 5 % B; 0.1–4.1 min: gradient to 95 % B; 4.1–6.1 min: 95 % B; 6.1–7.1 min: gradient to 5 % B; 7.1–13.1 min: 5 % B. The injection volume was 3 µl and the oven temperature was set at 40 °C. Detection was performed using an API4000 system (AB Sciex, France) in positive-ion mode with an electrospray ionization (ESI) source. Multiple reaction monitoring (MRM) transitions used for quantification were as follows: 255.1 > 84.2 for furosine and 259.0 > 88.2 for d_4-furosine.

CML quantification was performed using a LC20 chromatographic system (Shimadzu) equipped with a Kinetex HILIC column (100 × 4.6 mm, 2.6 µm - Phenomenex) with a gradient program composed of 5 mM ammonium formate (pH 2.9) as mobile phase A and 100 % acetonitrile as mobile phase B. The flow rate was constant at 0.9 ml/min during all separation steps. The gradient program was as follows: 0–0.3 min: 90 % B; 0.3–1.5 min: gradient to 50 % B; 1.5–2.0 min: 50 % B; 2.0–3.1 min: gradient to 40 % B; 3.1–3.5 min: 40 % B; 3.5–4.0 min: gradient to 90 % B. The injection volume was 10 µl and the oven temperature was set at 25 °C. Detection was performed using an API4000 system (AB Sciex, France) in positive-ion mode with an electrospray ionization (ESI) source. Multiple reaction monitoring (MRM) transitions used for quantification were as follows: 205.1 > 130.1 for CML and 207.1 > 84.1 for d_2-CML. Calibration curves were performed by preparing diluted serum solutions spiked with increased amounts of CML (ranging from 2.5 µM to 80 µM), which have been submitted to the same preanalytical treatments as patient samples. In addition, the lysine content in the hydrolysate was quantified by LC-MS/MS to normalise the expression of results.

2.1.4.3. Fluorescent AGE quantification. To quantify fluorescent AGEs present in the collagen of the bone, a fluorometric assay [30] was performed, using a similar approach to our previous study [28]. After the specimens had been mechanically tested, approximately 100 mg of each bone was demineralised in 45 % formic acid with a 1 mM sodium citrate buffer. Once the samples were demineralised, all that remained were the organic components from each sample. The collagen was digested in a papain digest solution of 3.88 units of papain in 0.1 mM sodium acetate buffer at 65 °C in an oven for 16 h. The samples were then centrifuged to separate the supernatant from any non-digested material. The papain digested samples were then hydrolysed by placing equal parts of the supernatant and HCL ~38 % into an Eppendorf and incubating at 100 °C for 18 h. The samples were then allowed to dry out and be rehydrated. To determine the fluorescent AGEs, the rehydrated samples were compared against a quinine standard of 0, 0.5, 1, 2, 3.5,5,10, and 20 µg/ml, which were made using a stock solution of 50 µg/ml quinine per 0.1 N sulfuric acid. 200 µl of each sample was carefully pipetted into a 96-well plate and a Biotek plate reader was used at 360/460 nm excitation/emission. A hydroxyproline assay was also carried out to determine the amount of collagen in each sample so that the nanograms of quinine per milligram of collagen could be calculated.

2.1.5. Statistical analyses

All statistical analyses were performed using GraphPad statistical software. Normality was tested using the Kolmogorov- Smirnov

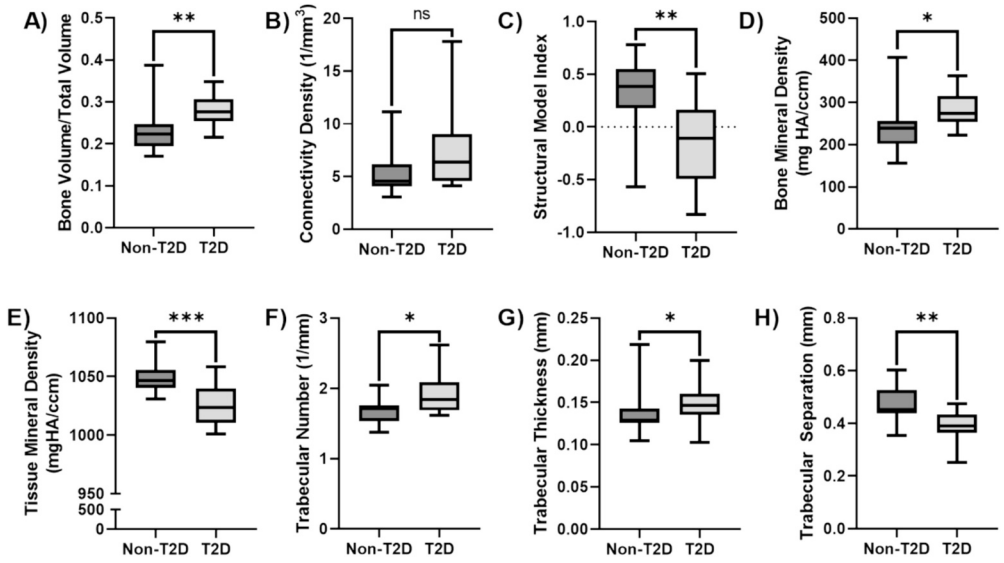

Fig. 4. Micro-CT results A) BV/TV, B) connectivity density, C) structural model index, D) bone mineral density, E) tissue mineral density, F) trabecular number, G) trabecular thickness, and H) trabecular separation. *($p < 0.05$), **($p < 0.01$), ***($p < 0.001$).

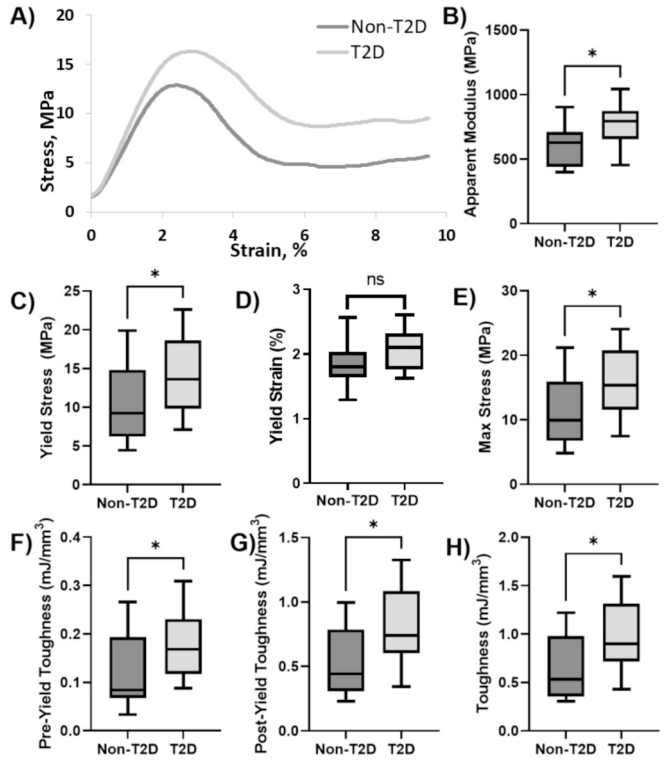

Fig. 5. Monotonic compression mechanical properties A) representative stress-strain curve, B) apparent modulus, C) yield stress, D) yield strain, E) max stress, F) pre-yield toughness, G) post-yield toughness, and H) toughness. *($p < 0.05$).

normality test. Two-sample *t*-tests were used to evaluate normally distributed data. A nonparametric Mann-Whitney was used to evaluate non-normally distributed data. In these analyses, the type 2 diabetic group was compared to the non-diabetic group. For all tests, $p < 0.05$, was considered statistically significant. Boxplots were prepared using GraphPad. The distribution of mechanical properties was analysed to detect potential outliers. Data from samples that were two standard deviations from the mean being removed. This resulted in a total of five samples being removed in the analysis (non-T2D ($n = 2$), and T2D ($n = 3$)). Additionally, insufficient cortical bone was present in some femoral heads from the femoral neck, leading to the following sample numbers for cortical bone analysis: T2D ($n = 14$) and non-T2D ($n = 14$) for nanoindentation and T2D ($n = 15$) and non-T2D ($n = 11$) for fluorescent AGE analysis, Raman, and LC-MS/MS results.

3. Results

3.1. Bone morphology

Fig. 4 shows the morphological properties determined through micro-CT scanning, with significant differences observed between the type 2 diabetic and non-diabetic samples for several parameters. Type 2 diabetic bone had significantly higher BV/TV (+22 %, $p = 0.008$), trabecular thickness (+7 %, $p = 0.026$) trabecular number (+13 %, $p = 0.016$), and bone mineral density (+18 %, $p = 0.027$) compared to non-diabetic controls. Type 2 diabetic bone had significantly lower tissue mineral density (−2 %, $p < 0.001$) and trabecular separation (−17 %, $p = 0.002$) compared to the non-diabetic controls. Type 2 diabetic bone had a significantly lower structural model index compared to non-diabetic. Here, the type 2 diabetic bone had a negative mean, which is indicative of a concave surface, while the non-diabetic bone had a positive mean, which is indicative of a convex surface. The SMI was also closer to zero for the type 2 diabetic group, meaning the structure was more plate-like compared to the non-diabetic group. There were no differences in connectivity density or trabecular thickness between groups.

3.2. Mechanical results

3.2.1. Monotonic loading

Type 2 diabetic and non-diabetic trabecular bone cores were tested under monotonic compression. A representative stress-strain curve is shown in Fig. 5A. Fig. 5B–H show boxplots of the mechanical properties that were evaluated across both groups. It was found that the type 2 diabetic samples had a significantly higher apparent modulus (+26 %, $p = 0.021$), yield stress (+39 %, $p = 0.026$), max stress (+47 %, $p = 0.012$), pre-yield toughness (+33 %, $p = 0.029$), post-yield toughness (+59 %, $p = 0.018$) and toughness (+56 %, $p = 0.016$) compared to the non-diabetic group, see Table 2. The results were normalised by BV/TV (as it is the best morphological determinant of bone stiffness [60,61]). When normalised against BV/TV (by dividing by BV/TV), all the

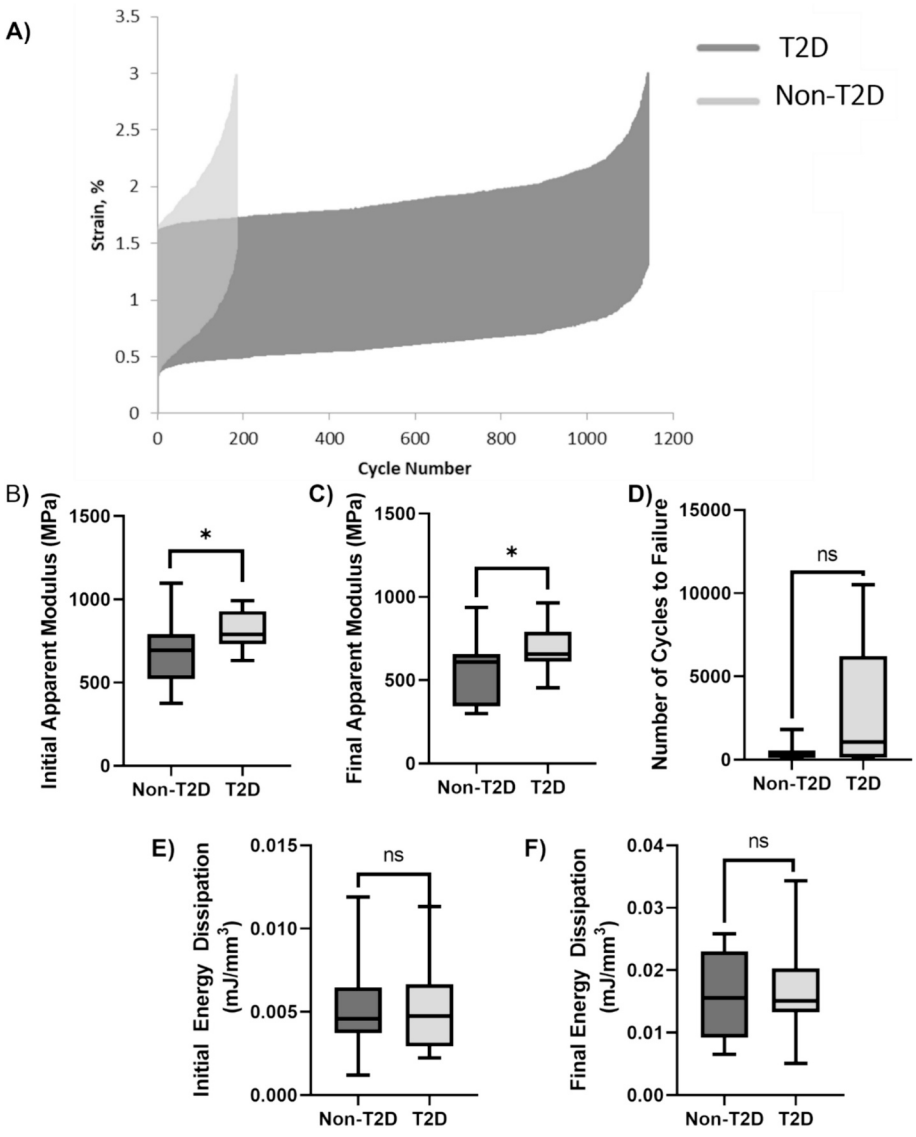

Fig. 6. Cyclic compression mechanical properties A) representative creep-fatigue curve, B) initial apparent modulus, C) final apparent modulus, D) number of cycles to failure, E) initial energy dissipation, and F) final energy dissipation. *($p < 0.05$).

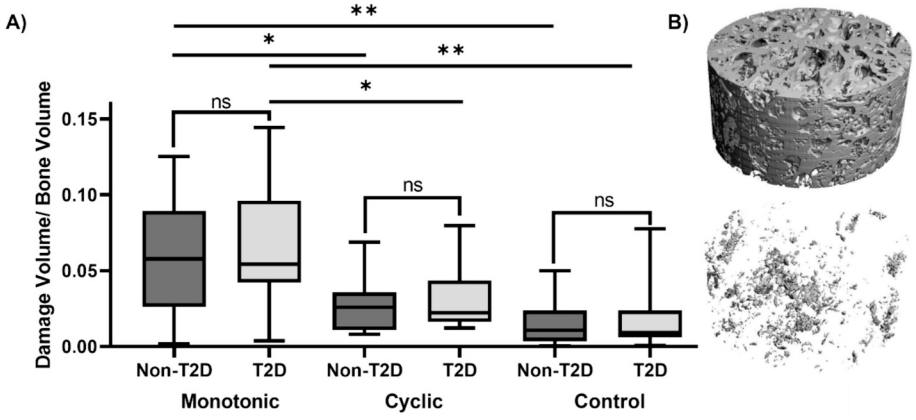

Fig. 7. Microdamage accumulation in the trabecular bone samples after the mechanical tests A) Microdamage ratio in the bone volume, B) image of the micro-CT scan of the staining of barium sulfate showing the damage. *($p < 0.05$), **($p < 0.01$).

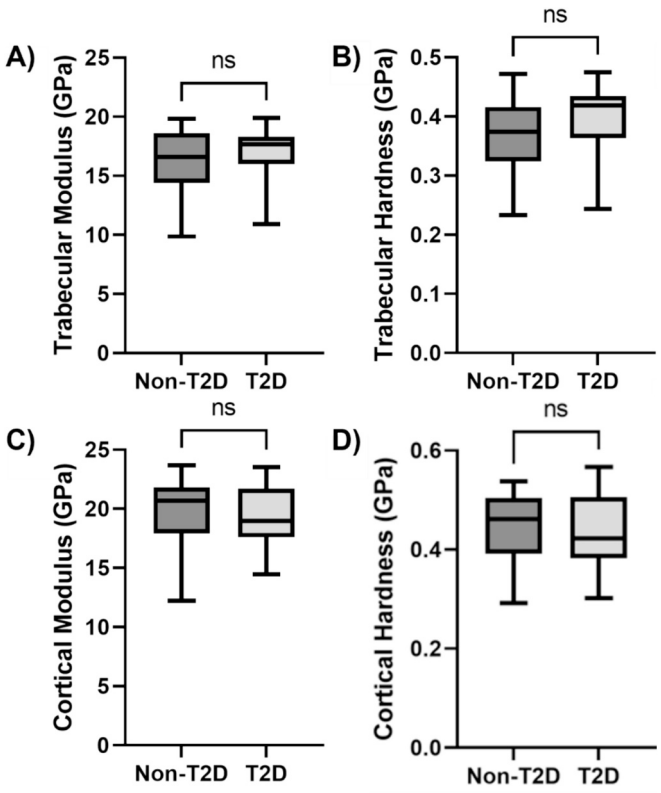

Fig. 8. Nanoindentation results A) trabecular modulus, B) trabecular hardness, C) cortical modulus, and D) cortical hardness.

previously significant properties remained significantly higher in the type 2 diabetic group compared to the non-diabetic. The data was also normalised using both a generalised linear model (GLM) and a power law model (PLM), which involved fitting a linear and power law trendline, respectively, to the data. These are both common ways to normalise mechanical properties when dealing with bone, to separate the effect of the porous structure. The equations of each trendline were then used to normalise the data using the GLM and PLM methods, respectively, resulting in the normalised GLM and PLM data, which are summarised in Table 3. After GLM and PLM normalisation, none of the properties remained significantly higher in the type 2 diabetic group.

3.2.1.1. Cyclic loading. Fig. 6A shows the creep-fatigue curve consisting of the primary, secondary, and tertiary phases of the creep response. Fig. 6B shows the cyclic mechanical properties. It was found that the type 2 diabetic group had higher initial modulus (+20 %, $p = 0.025$) and final modulus (+24 %, $p = 0.032$) compared to the non-diabetic group. There were no significant differences in the initial energy dissipation, final energy dissipation, or the number of cycles to failure when comparing the type 2 diabetic samples with the non-diabetic samples.

3.2.1.2. Microdamage accumulation. The microdamage accumulation volume across each group was labelled with barium sulfate precipitate to calculate the damage volume/bone volume (Fig. 7). There was no significant difference in the level of microdamage accumulation between type 2 diabetic and non-diabetic samples. However, there was a significant difference in the microdamage accumulation across the mechanical tests carried out. In the type 2 diabetic group, the monotonic compression sample had a significantly higher level of microdamage compared to the cyclic sample and the non-mechanically tested control sample. The same significant differences were present for the non-diabetic group, with the monotonic samples having a significantly higher level of microdamage accumulation than the cyclic and control samples. One non-diabetic sample was incorrectly stained during this process and was removed from the analysis.

3.2.1.3. Nanoindentation testing. Nanoindentation testing was performed on trabecular and cortical tissue (Fig. 8). No significant differences were found in either elastic modulus or hardness between the non-diabetic and type 2 diabetic groups in any of the cortical or trabecular regions examined.

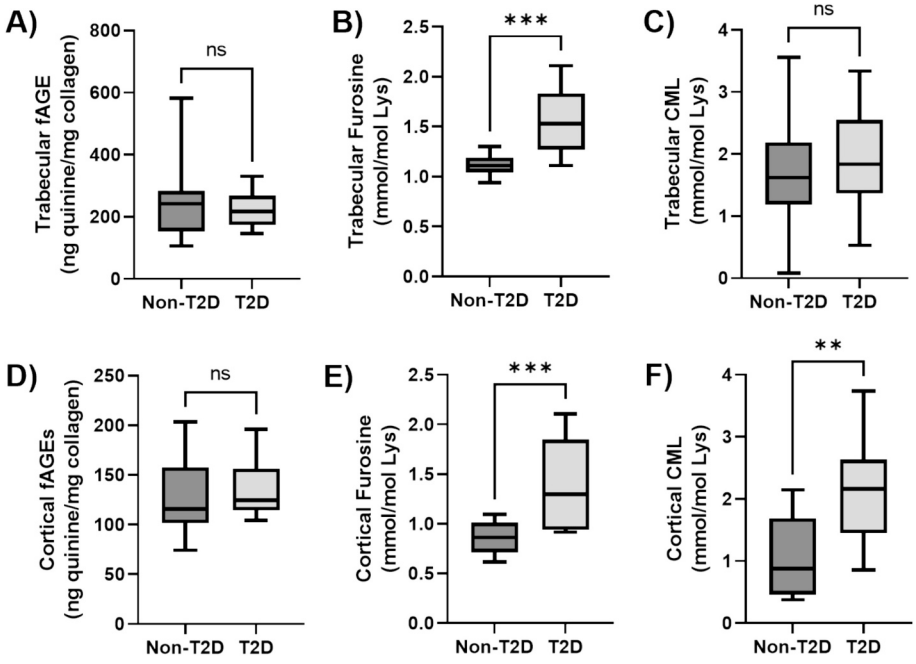

Fig. 9. Compositional analysis of bone A) trabecular fluorescent AGEs, B) trabecular furosine, C) trabecular CML, D) cortical fluorescent AGEs, E) cortical furosine, and cortical CML. *($p < 0.05$), **($p < 0.01$), ***($p < 0.001$).

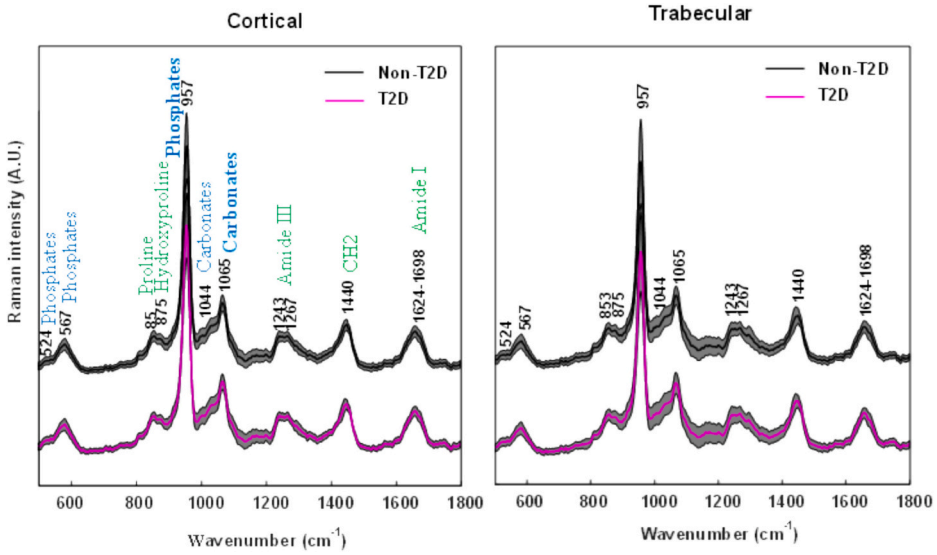

Fig. 10. Mean Raman spectra of non-diabetic and type 2 diabetic cortical and trabecular bone.

Table 1
Demographics of non-diabetic and type 2 diabetic patients enrolled in the study, where OP is osteoporosis and OA is osteoarthritis.

Demographics	Non-T2D	T2D
Sex	Female: 8 (7 OP, 1 OA) Male: 9 (1 OP, 8 OA)	Female: 8 (7 OP, 1 OA) Male: 9 (1 OP, 8 OA)
Age	74 ± 9 years	74 ± 9 years
Disease (OP/OA)	8 OP, 9 OA	8 OP, 9 OA
hBA1c	Not available	57.6 ± 14.2 mmol/mol (n = 10)

3.2.2. Compositional results

3.2.2.1. Fluorescent AGE analysis and LC-MS/MS. The results from the compositional analysis of bone are shown in Fig. 9 and Table 4. The results of the fluorescent AGE analysis are shown in Fig. 9A–C for cortical bone and Fig. 9D–F for trabecular bone. No differences were found in the levels of fluorescent AGE in cortical or trabecular bone of non-T2D compared to T2D. Levels of glycation were significantly higher in the type 2 diabetic compared to the non-diabetic group, with higher measurements of trabecular furosine (+40 %, $p < 0.001$), cortical furosine (+65 %, $p = 0.001$) and cortical CML (+97 %, $p = 0.004$), as shown in Fig. 9B, C and E respectively. Trabecular CML (+10 %, $p = 0.604$) was not significantly different.

3.2.2.2. Raman spectroscopy. The chemical composition of type 2 diabetic and non-diabetic cortical and trabecular bone was analysed using Raman spectroscopy. The spectra for both diabetic and non-diabetic bone exhibited characteristic Raman bands corresponding to the mineral and organic constituents of bone, see Fig. 10. The observed bands included a strong phosphate (PO4) bands at 524, 567, and 957 cm^{-1}, and carbonate (CO_3) bands at 1044 and 1065 cm^{-1}. Other bands were associated with the collagen matrix, including proline and hydroxyproline amino acid rings at 853 and 875 cm^{-1}, the amide III band (N—H bending and C—N stretching) at 1243 and 1267 cm^{-1}, CH_2 deformation bands of proteins at 1440 cm^{-1}, and the Amide *I* band dominated by carbonyl stretching vibration.

To investigate conformational changes in the secondary structure of collagen between type 2 diabetic and non-diabetic cortical and trabecular bone, the Amide *I* band was decomposed using curve-fitting analysis. This analysis revealed four sub-bands centered at 1624, 1653, 1674, and 1698 cm^{-1} assigned respectively to β-sheets, α-helices, random coil, and β-turns secondary structures of collagen. Statistical analysis, using analysis of variance ANOVA followed by pairwise Tukey test, was performed on the intensity ratios of Raman bands to identify significant changes between non-diabetic and type 2 diabetic cortical and trabecular bone. Statistical significance is represented with asterisks ($*p < 0.05$, $**p < 0.01$, $***p < 0.001$).

From these spectra, we calculated several parameters: mineral/matrix ratios such as PO_4/Amide *I* subbands (1624, 1653, 1674, and 1698 cm^{-1}), PO_4/Amide III (1243 and 1267 cm^{-1}), PO_4/Proline (853 cm^{-1}), and PO_4/CH_2,(1440 cm^{-1}) to quantify the relative content of mineral

Table 2
Trabecular bone monotonic compression and cyclic compression measured mechanical properties.

	Non-T2D (n = 15)	T2D (n = 14)	p-Value
Monotonic compression			
Apparent modulus (MPa)	605 ± 175	763 ± 171	**0.021**
Yield stress (MPa)	10.21 ± 4.7	14.19 ± 4.4	**0.026**
Yield strain (%)	1.87 ± 0.32	2.09 ± 0.32	0.075
Max stress (MPa)	10.98 ± 5.08	16.11 ± 5.15	**0.012**
Post-yield strain (%)	7.55 ± 0.54	7.31 ± 0.55	0.241
Pre-yield toughness (mJ/mm^3)	0.12 ± 0.07	0.16 ± 0.07	**0.029**
Post-yield toughness (mJ/mm^3)	0.51 ± 0.25	0.81 ± 0.32	**0.018**
Toughness (mJ/mm^3)	0.63 ± 0.32	0.98 ± 0.39	**0.016**
Mean intercept length tensor (°)	18.9 ± 12.4	12.9 ± 6.71	0.111
Cyclic compression			
Initial apparent modulus (MPa)	676 ± 188	814 ± 166	**0.025**
Final apparent modulus (MPa)	561 ± 187	695 ± 151	**0.042**
% Reduction in modulus	16.8 ± 17.6	15 ± 11.3	0.738
Initial energy dissipation (mJ/mm^3)	0.005 ± 0.003	0.005 ± 0.003	0.881
Final energy dissipation (mJ/mm^3)	0.016 ± 0.007	0.016 ± 0.007	0.885
% Increase in energy dissipation	262 ± 205	241 ± 206	0.791
Number of cycles to failure (N_f)	484 ± 553	2952 ± 3988	0.131

Table 3
Monotonic results normalised three ways, firstly by dividing by BV/TV, secondly by using a general linear model, and finally by using a power law model.

Normalised	Non-T2D ($n = 15$)	T2D ($n = 14$)	p-Value
Monotonic compression divided by BV/TV			
Apparent modulus (MPa/(BV/TV))	2633 ± 760	3320 ± 746	**0.021**
Yield stress (MPa/(BV/TV))	44.4 ± 20.4	61.8 ± 19.2	**0.026**
Max stress (MPa/(BV/TV))	47.8 ± 22.1	70.1 ± 22.4	**0.012**
Pre-yield toughness (mJ/mm^3)/(BV/TV)	0.50 ± 0.29	0.73 ± 0.30	**0.042**
Post-yield toughness (mJ/mm^3/(BV/TV))	2.21 ± 1.09	3.52 ± 1.41	**0.011**
Toughness (mJ/mm^3/(BV/TV))	2.71 ± 1.37	4.25 ± 1.68	**0.013**
General linear model			
Apparent modulus (MPa)	0.93 ± 0.20	1.07 ± 0.23	0.078
Yield stress (MPa)	0.91 ± 0.25	1.09 ± 0.32	0.110
Max stress (MPa)	0.88 ± 0.23	1.11 ± 0.36	0.073
Pre-yield toughness (mJ/mm^3)	0.90 ± 0.30	1.09 ± 0.42	0.166
Post-yield toughness (mJ/mm^3)	0.85 ± 0.21	1.13 ± 0.49	0.063
Toughness (mJ/mm^3)	0.86 ± 0.21	1.13 ± 0.47	0.067
Power law model			
Apparent modulus (MPa)	0.97 ± 0.20	1.08 ± 0.24	0.181
Yield stress (MPa)	0.97 ± 0.26	1.12 ± 0.36	0.198
Max stress (MPa)	0.95 ± 0.25	1.15 ± 0.41	0.128
Pre-yield toughness (mJ/mm^3)	0.98 ± 0.33	1.17 ± 0.46	0.211
Post-yield toughness (mJ/mm^3)	0.93 ± 0.23	1.19 ± 0.55	0.116
Toughness (mJ/mm^3)	0.93 ± 0.23	1.18 ± 0.52	0.118

Table 4
Compositional analysis of bone with results from LC-MS/MS and fluorometric analysis. fAGE = fluorescent AGE.

	Non-T2D	T2D	p-Value
Trabecular furosine (mmol/mol Lys)	1.12 ± 0.10	1.57 ± 0.33	**<0.001**
Trabecular CML (mmol/mol Lys)	1.78 ± 0.88	1.95 ± 0.80	0.604
Cortical furosine (mmol/mol Lys)	0.86 ± 0.16	1.42 ± 0.44	**0.001**
Cortical CML (mmol/mol Lys)	1.05 ± 0.66	2.07 ± 0.80	**0.004**
Trabecular fAGE ng quinine/mg collagen	255.0 ± 127.0	226.6 ± 58.6	0.444
Cortical fAGE ng quinine/mg collagen	128.5 ± 39.6	135.3 ± 29.7	0.665

(phosphate or carbonate) to organic (collagen) components within bone, carbonate substitution (CO_3/PO_4) to provide information on the changes in the bone mineral composition, mineral crystallinity using the full width at half maximum (FWHM) of the phosphate (PO_4) band at 957 cm^{-1}. Collagen quality was evaluated using the matrix maturity ratio (1674/1698), helical status (1674/1653), Hyp/Proline ratio, and Amide *I* subbands/Amide III bands ratio. The results are presented in Table 5.

The mineral/matrix ratios showed significant differences between type 2 diabetic and non-diabetic groups in both trabecular and cortical bone. Type 2 diabetic trabecular bone exhibited significantly higher mineral/matrix ratios compared to non-diabetic trabecular bone. In addition, PO_4/amide I sub-band ratios were on average higher in both non-diabetic and type 2 diabetic trabecular bone compared to cortical bone. Type 2 diabetic trabecular bone exhibited significantly higher mineral/matrix ratios compared to non-diabetic: $PO_4/1653$ and $PO_4/1698$ (+63 % and 43 % respectively, $p < 0.001$), $PO_4/1267$ (+27 %, $p < 0.001$), $PO_4/853$ (+53 %, $P < 0.001$), and $PO_4/1440$ (+19 %, $p < 0.001$). Additionally, from carbonate/amide I sub-bands, $CO_3/1653$ was the only ratio significantly higher in type 2 diabetic compared to non-diabetic trabecular bone (+24 %, $p > 0.001$), while $CO_3/1674$ was lower in the type 2 diabetic compared to non-diabetic trabecular bone (−11 %, $p < 0.05$). In cortical bone, the only significant change observed was a lower 957/1624 ratio when comparing the type 2 diabetic to the non-diabetic group (−19 %, $p < 0.001$). The carbonate/amide I sub-bands ratios did not show any significant differences between non-diabetic and type 2 diabetic cortical bone. These ratios provide insights into bone mineralisation and collagen content, which are important for understanding bone quality and mechanical properties. In cortical bone, the carbonate substitution PO_4/CO_3 ratio was higher by 14 % ($p < 0.001$) in the type 2 diabetic group, indicating a higher carbonate content into the bone mineral. Conversely, in trabecular bone, the carbonate substitution ratio was lower by 15 % ($p < 0.001$) in the type 2 diabetic group, suggesting a reduced carbonate content within the mineral phase. We also compared mineral crystallinity non-diabetic and type 2 diabetic groups for both cortical and trabecular bone. Our results revealed that T2D affected bone crystallinity differently in cortical and trabecular bone. In fact, there were no significant differences in the FWHM of the band at 957 cm^{-1} between non-diabetic and type 2 diabetic in either the cortical or trabecular bone. However, the intensity of this band was significantly lower in the type 2 diabetic compared to non-diabetic trabecular bone while cortical bone did not show any significant differences between the groups.

The matrix maturity and helical status ratios were calculated using the intensity ratios 1674/1698 and 1674/1698 respectively. Trabecular bone showed higher matrix maturity and helical status on average compared to cortical bone, with no significant differences observed between non-diabetic and type 2 diabetic groups. The Hyp/Proline ratio was used to evaluate the quality and stability of the collagen matrix in bone. A significantly higher Hyp/Proline ratio was observed in type 2 diabetic compared to non-diabetic cortical bone (+26 %, $p < 0.001$). This ratio did not show significant differences between groups in trabecular bone. The Amide *I*/Amide III ratios were used to investigate the organisation of the collagen matrix between non-diabetic and type 2 diabetic groups in cortical and trabecular bone. The amide I/amide III ratios of both non-diabetic and type 2 diabetic cortical bone were on average higher in than the corresponding trabecular bone. In addition, this ratio did not show significant differences when comparing non-diabetic and type 2 diabetic cortical bone. However, for trabecular bone, we observed significantly higher ratios of 1624/1267 cm^{-1} and 1674/1267 cm^{-1} (9 % and 23 %, respectively, $p < 0.001$). Overall, these results highlight the effect of T2D on the bone mineral and matrix properties in both cortical and trabecular bone.

4. Discussion

Previous population-level studies have found that type 2 diabetic patients have an increased fracture risk when compared to non-diabetic patients. The present study evaluated bone composition, mechanical properties, and microdamage accumulation of type 2 diabetic femoral head trabecular bone tissue under monotonic and cyclic loading and has added more information to the limited experimental data on human type 2 diabetic bone. It was found that T2D does not have a detrimental effect on the mechanical properties of trabecular bone from the femoral head of T2D patients. In fact, type 2 diabetic bone had higher strength, and resistance to deformation, with higher apparent modulus, yield stress,

Table 5
Cortical and trabecular bone compositional properties determined by Raman spectroscopy. Hyp is hydroxyproline (*$p < 0.05$, **$p < 0.01$, ***$p < 0.001$).

				Cortical			Trabecular		
Phase			Bands (cm^{-1})	Non-T2D	T2D	Non-T2D vs T2D	Non-T2D	T2D	Non-T2D vs T2D
Mineral phase/ organic phase	Mineral/matrix ratio	PO_4/Amide I	957/1624	0.21 ± 0.06	0.17 ± 0.04	(↓19 %) ***	0.25 ± 0.07	0.29 ± 0.07	NS
			957/1653	0.49 ± 0.14	0.42 ± 0009	NS	0.81 ± 0.28	1.32 ± 0.35	(↑63 %) ***
			957/1674	0.26 ± 0.07	0.26 ± 0.06	NS	0.35 ± 0.10	0.32 ± 0.09	NS
			957/1698	0.31 ± 0.09	0.33 ± 0.08	NS	0.51 ± 0.15	0.73 ± 0.19	(↑43 %) ***
		PO_4/Amide III	957/1243	0.72 ± 0.15	0.74 ± 0.02	NS	0.67 ± 0.14	0.72 ± 0.14	NS
			957/1267	0.22 ± 0.05	0.21 ± 0.04	NS	0.30 ± 0.08	0.44 ± 0.10	(↑27 %) ***
		PO_4/Proline	957/853	1.77 ± 0.44	2.18 ± 0.58	(↑23 %)**	1.5 ± 0.35	2.14 ± 0.55	(↑53 %) ***
		PO_4/CH_2	957/1440	0.28 ± 0.07	0.36 ± 0.08	(↑29 %) ***	0.31 ± 0.08	0.37 ± 0.09	(↑19 %) ***
		CO_3/Amide I	1065/1624	0.65 ± 0.08	0.60 ± 0.07	NS	0.74 ± 0.09	0.69 ± 0.10	NS
			1065/1653	1.89 ± 0.27	1.84 ± 0.31	NS	2.63 ± 0.44	3.27 ± 0.62	(↑24 %) ***
			1065/1674	1.03 ± 0.14	0.94 ± 0.14	NS	1.10 ± 0.15	0.97 ± 0.16	(↓11 %)**
			1065/1698	1.14 ± 0.17	1.25 ± 0.18	NS	1.77 ± 0.33	1.60 ± 0.25	NS
Mineral phase	Carbonate substitution	CO_3/PO_4	1065/957	2.95 ± 0.67	3.36 ± 0.68	(↑14 %) ***	2.74 ± 0.56	2.32 ± 0.46	(↓15 %) ***
	Crystallinity	PO_4	957 (intensity)	32.76 ± 11.0	33,01 ± 1.00	NS	29.99 ± 1.14	28.40 ± 1.06	(↓5 %)***
			957 (FWHM)	24.99 ± 0.43	25.00 ± 0.4	NS	25.45 ± 0.42	25.67 ± 0.45	NS
Organic phase	Matrix maturity	Amide sub band ratios	1674/1698	1.13 ± 0.21	1.09 ± 0.21	NS	1.31 ± 0.31	1.40 ± 0.31	NS
	Helical status		1674/1653	1.75 ± 0.29	1.68 ± 0.32	NS	2.49 ± 0.63	2.62 ± 0.58	NS
	Hyp to proline		875/853	7.33 ± 1.84	9.24 ± 2.31	(↑26 %) ***	4.37 ± 0.92	4.78 ± 1.00	NS
	Amide I/Amide III		1624/1243	2.69 ± 0.61	3.21 ± 1.04	NS	1.82 ± 0.38	1.84 ± 0.41	NS
			1653/1243	1.01 ± 0.33	1.10 ± 0.38	NS	0.41 ± 0.14	0.44 ± 0.13	NS
			1674/1243	1.84 ± 0.48	1.94 ± 0.67	NS	1.43 ± 0.37	1.30 ± 0.33	NS
			1698/1243	1.33 ± 0.37	1.61 ± 0.55	NS	0.82 ± 0.25	0.80 ± 0.22	NS
			1624/1267	1.38 ± 0.10	1.41 ± 0.13	NS	1.38 ± 0.13	1.50 ± 1.18	(↑9 %)***
			1653/1267	0.45 ± 0.05	0.46 ± 0.06	NS	0.32 ± 0.07	0.30 ± 0.06	NS
			1674/1267	0.84 ± 0.09	0.82 ± 0.12	NS	0.81 ± 0.13	1.00 ± 0.17	(↑23 %) ***
			1698/1267	0.66 ± 0.11	0.66 ± 0.08	NS	0.55 ± 0.10	0.56 ± 0.11	NS

max stress, pre- and post-yield toughness, and toughness. These findings are similar to the majority of other recent studies that have found no reduction in mechanical properties of type 2 diabetic trabecular bone [29,30,33] compared to non-diabetic controls. Furthermore, under cyclic loading, there were no significant differences in the number of cycles-to-failure, compared to controls. While elevated levels of AGEs were found in type 2 diabetic bone, along with distinct changes in the mineral-to-matrix ratio, mineral phase, and organic phase, it was found that T2D does not impair the mechanical properties of trabecular bone from the femoral heads of T2D patients. This suggests that other mechanisms may be responsible for the increased fracture risk seen in T2D patients.

These results are broadly in line with earlier research showing that T2D patients have either a denser or preserved trabecular microarchitecture compared to non-diabetic controls [29,42,62–64]. Structural analysis revealed a greater bone volume, trabecular thickness, and trabecular number in the type 2 diabetic samples compared to non-diabetic samples, although lower tissue mineral density and trabecular separation were found in the type 2 diabetic samples, while connectivity density was not significantly different. Other studies have found denser or maintained trabecular microarchitecture in populations with predominantly well-controlled or early-stage T2D [42,62]. However, longer disease duration or the presence of comorbidities can result in impaired microarchitecture, with reductions in bone volume fraction reported in T2D patients who have undergone a fragility fracture with a mean duration of disease of 7.5 years [31]. The preserved trabecular microarchitecture in T2D could be a result of an anabolic reaction brought on by hyperinsulinemia [65], remodelling adjustment to higher BMI, or the altered remodelling process seen in T2D. In the current study, the BMI of the T2D patients was unfortunately not available. However, generally, patients with T2D tend to have higher BMI compared to people in good health [64].

Raman spectroscopy indicated that the composition of the bone matrix was altered in the type 2 diabetic group compared to the non-diabetic bone. The type 2 diabetic trabecular bone had a higher mineral-to-matrix ratio, a lower carbonate substitution, and crystallinity compared to the non-diabetic trabecular bone. These compositional changes could be, in part, linked to the altered mechanical properties in type 2 diabetic trabecular bone found in this study. Higher mineral-to-matrix ratio has been linked to higher strength in cortical bone [66,67] so this could contribute to the higher effective strength of the trabecular samples obtained here under monotonic loading. However, it should be noted that if the bone becomes too mineralised, it can become brittle and be more likely to fracture. The precise role of both carbonate substitution and crystallinity and their effect on the mechanical properties of bone remains poorly understood [67]. Some studies have found that higher carbonate substitution was linked to reduced strength [67] and fragility [68], while others have found that lower carbonate substitution was linked to fragility [69]. Higher crystallinity has also been linked with increased strength [67] and stiffness and decreased ductility [70], suggesting lower crystallinity would lead to the opposite. However, despite the type 2 diabetic group having lower crystallinity there was no reduction in mechanical properties. Additionally, the differences in mineral-to-matrix ratio, carbonate substitution, and crystallinity

suggest an altered remodelling process is occurring in T2D compared to non-T2D. Studies that investigated the bone tissue composition of T2D patients using different methods found varying results, with several studies finding no difference in compositional features [71,72] Other studies have observed different matrix composition. Sihota et al. [31] used FTIR and found a lower mineral-to-matrix ratio and enzymatic crosslink ratio, and a higher non-enzymatic crosslink ratio in T2D patients. Rokidi et al. [73] also used Raman and found no difference in the mineral-to-matrix ratio but an increase in mineral crystallinity in T2D patients compared to non-T2D controls. Rodic et al. [74] used Raman and found a higher carbonate substitution in the cortical bone of the buccal cortex of T2D patients but no difference in the mineral-to-matrix ratio. Further research is needed to elucidate the precise compositional characteristics of type 2 diabetic bone.

Bulk measurement of total fluorescent AGEs revealed no significant differences between T2D and non-T2D, which is similar to findings across several recent studies that have also measured bulk fluorescent AGEs [29,30]. However, other studies have found differences in bulk fluorescent AGE accumulation [31,62,75]. In the current study, there were significant changes in non-fluorescent AGEs in type 2 diabetic bone, reporting for the first time higher levels of furosine present in cortical and trabecular bone, while also observing higher levels of CML in cortical bone, which has been shown previously [73,76]. Recently, Arakawa and colleagues found that, of the AGEs that are currently quantifiable, adducts are considerably more abundant than crosslinks by at least an order of magnitude [77]. This highlights the importance of measuring not only the bulk fluorescent AGEs but also specific non-fluorescent and adduct AGEs such as CML.

Under monotonic loading, it was found that the apparent modulus, yield stress, maximum stress, pre-yield toughness, post-yield toughness, and toughness were significantly greater for the type 2 diabetic trabecular samples compared to the non-diabetic samples. In the present study, multiple normalisation methods were used to provide a comprehensive analysis and to highlight how different approaches can influence the interpretation of the data. When normalised by dividing by the respective bone volume fraction, the max stress, pre-yield toughness, post-yield toughness, and toughness remained significantly higher. These results suggest that the type 2 diabetic samples had improved tissue-level properties, with higher strength and resistance to deformation. However, it should be noted these significant differences were no longer evident when normalised using GLM and PLM. This indicates that the variation in bone density is a major contributing factor to the observed mechanical differences. These findings are similar to those of Hunt et al. [29] who found a higher modulus, yield stress, and ultimate stress in type 2 diabetic samples at the apparent level that remained higher when normalised by bone volume fraction, although the post-yield properties did not differ across groups. Several other studies [30,75] have found no differences in the apparent mechanical properties of type 2 diabetic bone. Another study [31] found impaired apparent level properties along with a lower bone volume fraction in the type 2 diabetic group. Similarly, the results from cyclic testing of the bone revealed that the initial apparent modulus and the final modulus were higher for the type 2 diabetic samples. There was no difference in the percentage reduction in modulus between the first and final cycles, nor were there differences between the initial or final energy dissipation or strain energies. Interestingly, this current study found that the number of cycles to failure for type 2 diabetic samples were not significantly different compared to non-diabetic samples this is despite the greater toughness found in the type 2 diabetic monotonic samples. However, reconciling the cyclic and monotonic loading results requires considering the differences in these tests and what they measure. The cyclic test measures how many repeated loads the material can withstand before failure. It focuses on fatigue properties and microstructural damage accumulation. The monotonic test, on the other hand, measures how much energy the material can absorb under a single, continuously increasing load. This reflects overall toughness and the material's resistance to crack initiation and propagation. The overall microdamage accumulation volume between groups was similar for all loading scenarios. Sacher et al. [42] also found that total damage accumulation did not differ in type 2 diabetic samples compared to non-diabetic samples following monotonic testing. Nanoindentation results fell within the range reported for human trabecular and cortical bone at the femoral neck [78], but no differences in tissue-level properties were observed. This finding is in line with a recent study [79] that also found no differences between type 2 diabetic and non-diabetic cortical bone using nanoindentation. Other studies have found impaired tissue-level mechanical properties through nanoindentation [31] and cyclic reference point indentation [30]. This may be explained by the fact that the cohort used in Sihota and colleagues' study consisted of first fragility fracture patients and the different test method used by Karim and colleagues. While AGE accumulation is hypothesised to cause increased fracture risk in T2D patients, no supporting evidence of this was found, with no significant difference in microdamage accumulation between groups. These changes coincided with higher mechanical properties under both monotonic and cyclic loading. Currently, there is a lack of in vivo and ex vivo human experimental evidence that quantitatively links AGE accumulation to increased bone fragility in T2D. Given these findings, there is still much to be understood about AGEs and their effects on bone, and, in particular, the impact that AGE adducts have on the mechanical properties of bone needs to be better understood [18]. This understanding needs to apply to both cortical and trabecular bone as they both play an important role in resisting fracture [80,81], particularly as it has been suggested that cortical bone may be primarily responsible for hip fractures that occur in the femoral neck [82].

There are some limitations associated with this study. The primary limitation of the study was the patient data information, which had limited information on factors such as BMI, HbA1C, disease duration, and long-term disease management. Fracture risk is influenced by T2D disease control and duration and therefore the results cannot be related to control or duration. While the results of this study are not controlled for disease control or duration, the samples came from sex, age, and disease-matched individuals with (clinically diagnosed osteoporosis) and without fractures (clinically diagnosed osteoarthritis), for details see Table 1. While the samples were disease-matched, the disease severity of the osteoporosis and osteoarthritis was not a metric that was captured. Another limitation is that bone from the femoral head was used instead of the femoral neck, which is a more common fracture site. This was done to ensure the results were comparable as not all explants had sufficient tissue in the femoral neck to extract samples. Finally, the applied cyclic strain was higher than physiological strain [83], however they are still below levels of uniaxial yield strain [84]. By using the selected strain range it was possible to induce detectable microdamage while preventing excessive degradation of the material caused by external environmental factors. This is the first study to report an increase in the early AGE marker furosine in type 2 diabetic bone. This study is also the first to characterise the cyclic behaviour and subsequent microdamage accumulation of type 2 diabetic bone.

5. Conclusions

This study complements the increasing body of recent research on the biomechanics of type 2 diabetic trabecular bone. It was found that the mechanical properties of trabecular bone from the femoral head of T2D patients were not impaired by the condition. In fact, type 2 diabetic bone had higher yield and maximum strength and greater resistance to deformation compared to controls, despite significantly greater levels for some AGEs. Distinct changes were observed in both the organic and mineral phases of the bone tissue matrix through compositional analysis, including a higher mineral-to-matrix ratio, a lower carbonate substitution, and crystallinity. These changes were found to correspond with higher mechanical properties under monotonic loading. These results are consistent with earlier investigations that also found no significant

reduction in mechanical properties of trabecular bone from patients with T2D. According to this study, T2D does not impair the mechanical properties of trabecular bone in the femoral head, suggesting that other processes may be responsible for the increased risk of fractures in T2D.

CRediT authorship contribution statement

Marissa Britton: Writing – review & editing, Writing – original draft, Visualization, Methodology, Investigation, Formal analysis, Data curation. **Genna E. Monahan:** Writing – review & editing, Investigation, Formal analysis. **Colin G. Murphy:** Writing – review & editing, Methodology, Investigation. **Stephen R. Kearns:** Writing – review & editing, Methodology, Investigation. **Aiden T. Devitt:** Writing – review & editing, Methodology, Investigation. **Anaïs Okwieka:** Writing – review & editing, Methodology. **Stéphane Jaisson:** Writing – review & editing, Methodology, Investigation. **Laurence Van Gulick:** Writing – review & editing, Methodology. **Abdelilah Beljebbar:** Writing – review & editing, Investigation. **Halima Kerdjoudj:** Writing – review & editing, Supervision, Resources, Project administration, Investigation, Funding acquisition, Conceptualization. **Jessica Schiavi:** Writing – review & editing, Supervision, Investigation, Funding acquisition. **Ted J. Vaughan:** Writing – review & editing, Supervision, Resources, Project administration, Funding acquisition, Conceptualization.

Declaration of competing interest

The authors declare no conflict of interest.

Data availability

Data will be made available on request.

Acknowledgements

This project has received funding from the European Research Council (ERC) under the EU's Horizon 2020 research and innovation program (Grant agreement No. 804108) and by the Irish Research Council Ulysses 2020 award scheme. The authors also acknowledge scientific and technical assistance of David Connolly and clinical input of Prof. John Carey.

References

[1] M. Janghorbani, et al., Systematic review of type 1 and type 2 diabetes mellitus and risk of fracture, Am. J. Epidemiol. 166 (5) (2007) 495–505.
[2] S. Epstein, D. LeRoith, Diabetes and fragility fractures - a burgeoning epidemic?, in: Bone, 2008.
[3] A.V. Schwartz, Diabetes mellitus: does it affect bone? Calcif. Tissue Int. 73 (6) (2003) 515–519.
[4] A.V. Schwartz, D.E. Sellmeyer, Diabetes, fracture, and bone fragility, Curr. Osteoporos. Rep. 5 (3) (2007) 105–111.
[5] L.J. Melton, et al., Fracture risk in type 2 diabetes: update of a population-based study, J. Bone Miner. Res. 23 (8) (2008) 1334–1342.
[6] W.D. Leslie, et al., Type 2 diabetes and bone, J. Bone Miner. Res. 27 (11) (2012) 2231–2237.
[7] V.V. Shanbhogue, et al., Type 2 diabetes and the skeleton: new insights into sweet bones, Lancet Diabetes Endocrinol. 4 (2) (2016) 159–173.
[8] E.S. Strotmeyer, et al., Diabetes is associated independently of body composition with BMD and bone volume in older white and black men and women: the health, aging, and body composition study, J. Bone Miner. Res. 19 (7) (2004) 1084–1091.
[9] S.A. Paschou, et al., Type 2 diabetes and osteoporosis: a guide to optimal management, J. Clin. Endocrinol. Metab. 102 (10) (2017) 3621–3634.
[10] N. Mercer, et al., Regulation of advanced glycation end product (AGE) receptors and apoptosis by AGEs in osteoblast-like cells, Mol. Cell. Biochem. 306 (1) (2007) 87–94.
[11] R. Sanguineti, et al., Pentosidine effects on human osteoblasts in vitro, in: Annals of the New York Academy of Sciences, Blackwell Publishing Inc., 2008.
[12] A.D. McCarthy, et al., Advanced glycation endproducts interfere with integrin-mediated osteoblastic attachment to a type-I collagen matrix, Int. J. Biochem. Cell Biol. 36 (5) (2004) 840–848.
[13] U. Valcourt, et al., Non-enzymatic glycation of bone collagen modifies osteoclastic activity and differentiation, J. Biol. Chem. 282 (8) (2007) 5691–5703.
[14] F. Sassi, et al., Type 2 diabetes affects bone cells precursors and bone turnover, BMC Endocr. Disord. 18 (1) (2018) 1–8.
[15] D. Purnamasari, et al., Low bone turnover in premenopausal women with type 2 diabetes mellitus as an early process of diabetes-associated bone alterations: a cross-sectional study, BMC Endocr. Disord. 17 (1) (2017) 1–8.
[16] M. Ghodsi, et al., Mechanisms involved in altered bone metabolism in diabetes: a narrative review, J. Diabetes Metab. Disord. 15 (2016) 52.
[17] G.E. Monahan, et al., Longitudinal alterations in bone morphometry, mechanical integrity and composition in Type-2 diabetes in a Zucker diabetic fatty (ZDF) rat, Bone 170 (2023) 116672.
[18] T.L. Willett, P. Voziyan, J.S. Nyman, Causative or associative: a critical review of the role of advanced glycation end-products in bone fragility, Bone 163 (2022) 116485.
[19] S. Khosla, et al., Update on the pathogenesis and treatment of skeletal fragility in type 2 diabetes mellitus, Nat. Rev. Endocrinol. 17 (11) (2021) 685–697.
[20] V. Carnevale, et al., Bone damage in type 2 diabetes mellitus, Nutr. Metab. Cardiovasc. Dis. 24 (11) (2014) 1151–1157.
[21] M. Unal, et al., Effect of ribose incubation on physical, chemical, and mechanical properties of human cortical bone, J. Mech. Behav. Biomed. Mater. 140 (2023) 105731.
[22] D. Vashishth, et al., Influence of nonenzymatic glycation on biomechanical properties of cortical bone, Bone 28 (2) (2001) 195–201.
[23] S.Y.Y. Tang, U. Zeenath, D. Vashishth, Effects of non-enzymatic glycation on cancellous bone fragility, Bone 40 (4) (2007) 1144–1151.
[24] S. Viguet-Carrin, et al., An in vitro model to test the contribution of advanced glycation end products to bone biomechanical properties, Bone 42 (1) (2008) 139–149.
[25] T.L. Willett, et al., In vitro non-enzymatic ribation reduces post-yield strain accommodation in cortical bone, Bone 52 (2) (2013) 611–622.
[26] S. Jia, et al., Influence of non-enzymatic glycation on the mechanical properties of cortical bone, J. Mech. Behav. Biomed. Mater. 119 (2021) 104553.
[27] K. Merlo, et al., In vitro-induced high sugar environments deteriorate human cortical bone elastic modulus and fracture toughness, J. Orthop. Res. 38 (5) (2020) 972–983.
[28] M. Britton, E. Parle, T. Vaughan, An investigation on the effects of in vitro induced advanced glycation end-products on cortical bone fracture mechanics at fall-related loading rates, J. Mech. Behav. Biomed. Mater. (2022) 105619.
[29] H.B. Hunt, et al., Altered tissue composition, microarchitecture, and mechanical performance in cancellous bone from men with type 2 diabetes mellitus, J. Bone Miner. Res. (2019) (p. jbmr.3711-jbmr.3711).
[30] L. Karim, et al., Bone microarchitecture, biomechanical properties, and advanced glycation end-products in the proximal femur of adults with type 2 diabetes, Bone 114 (2018) 32–39.
[31] P. Sihota, et al., Investigation of mechanical, material and compositional determinants of human trabecular bone quality in type 2 diabetes, J. Clin. Endocrinol. Metab. XX (2021) 1–19.
[32] D.H. Yang, et al., Increased levels of circulating advanced glycation end-products in menopausal women with osteoporosis, Int. J. Med. Sci. 11 (5) (2014) 453–460.
[33] E. Parle, et al., Bone mineral is more heterogeneously distributed in the femoral heads of osteoporotic and diabetic patients: a pilot study, JBMR Plus 4 (2) (2020) e10253.
[34] C.J. Hernandez, T.M. Keaveny, A biomechanical perspective on bone quality, in: Bone, NIH Public Access, 2006, pp. 1173–1181.
[35] M.B. Schaffler, K. Choi, C. Milgrom, Aging and matrix microdamage accumulation in human compact bone, Bone 17 (6) (1995) 521–525.
[36] S. Mori, et al., Trabecular bone volume and microdamage accumulation in the femoral heads of women with and without femoral neck fractures, Bone 21 (6) (1997) 521–526.
[37] N.L. Fazzalari, et al., Three-dimensional confocal images of microdamage in cancellous bone, Bone 23 (4) (1998) 373–378.
[38] N.L. Fazzalari, et al., Assessment of cancellous bone quality in severe osteoarthrosis: bone mineral density, mechanics, and microdamage, Bone 22 (4) (1998) 381–388.
[39] S. Mori, D.B. Burr, Increased intracortical remodeling following fatigue damage, Bone 14 (2) (1993) 103–109.
[40] D.B. Burr, et al., Bone remodeling in response to in vivo fatigue microdamage, J. Biomech. 18 (3) (1985) 189–200.
[41] O.D. Kennedy, et al., Osteocyte apoptosis is required for production of osteoclastogenic signals following bone fatigue in vivo, Bone 64 (2014) 132–137.
[42] S.E. Sacher, et al., Distributions of microdamage are altered between trabecular rods and plates in cancellous bone from men with type 2 diabetes mellitus, J. Bone Miner. Res. 37 (4) (2022) 740–752.
[43] S.Y.Y. Tang, D. Vashishth, Non-enzymatic glycation alters microdamage formation in human cancellous bone, Bone 46 (1) (2010) 148–154.
[44] M.C. Michel, W.C. Hayes, Fatigue Behavior of vol. 26(907), 1993.
[45] T.L.A. Moore, L.J. Gibson, Fatigue of bovine trabecular bone, J. Biomech. Eng. 125 (6) (2003) 761–768.
[46] F.M. Lambers, et al., Microdamage caused by fatigue loading in human cancellous bone: relationship to reductions in bone biomechanical performance, PLoS One 8 (12) (2013) 1–9.
[47] M. Ryan, et al., A new approach to comprehensively evaluate the morphological properties of the human femoral head: example of application to osteoarthritic joint, Sci. Rep. 10 (1) (2020) 5538.
[48] G. Bevill, F. Farhamand, T.M. Keaveny, Heterogeneity of yield strain in low-density versus high-density human trabecular bone, J. Biomech. 42 (13) (2009) 2165–2170.

[49] J.O. Green, et al., Age-related differences in the morphology of microdamage propagation in trabecular bone, J. Biomech. 44 (15) (2011) 2659–2666.
[50] S. Hengsberger, A. Kulik, P. Zysset, Nanoindentation discriminates the elastic properties of individual human bone lamellae under dry and physiological conditions, Bone 30 (1) (2002) 178–184.
[51] E. Mittra, S. Akella, Y.-X. Qin, The effects of embedding material, loading rate and magnitude, and penetration depth in nanoindentation of trabecular bone, J. Biomed. Mater. Res. A 79A (1) (2006) 86–93.
[52] L. Mulder, et al., Intratrabecular distribution of tissue stiffness and mineralization in developing trabecular bone, Bone 41 (2) (2007) 256–265.
[53] O. Brennan, et al., Biomechanical properties across trabeculae from the proximal femur of normal and ovariectomised sheep, J. Biomech. 42 (4) (2009) 498–503.
[54] L. O'Sullivan, Time-Sequence of Biomechanical Adaption in Trabecular Tissue During Estrogen Deficiency, 2020.
[55] M.D. Landrigan, et al., Contrast-enhanced micro-computed tomography of fatigue microdamage accumulation in human cortical bone, Bone 48 (3) (2011) 443–450.
[56] X. Wang, et al., Detection of trabecular bone microdamage by micro-computed tomography, J. Biomech. 40 (15) (2007) 3397–3403.
[57] L. Van Gulick, et al., An integrated approach to investigate age-related modifications of morphological, mechanical and structural properties of type I collagen, Acta Biomater. 137 (2022) 64–78.
[58] E. Schleicher, L. Scheller, O.H. Wieland, Quantitation of lysine-bound glucose of normal and diabetic erythrocyte membranes by HPLC analysis of furosine [ε-N(L-furoylmethyl)-L-lysine], Biochem. Biophys. Res. Commun. 99 (3) (1981) 1011–1019.
[59] D.R. Sell, Ageing promotes the increase of early glycation Amadori product as assessed by ε-N-(2-furoylmethyl)-l-lysine (furosine) levels in rodent skin collagen: the relationship to dietary restriction and glycoxidation, Mech. Ageing Dev. 95 (1–2) (1997) 81–99.
[60] G. Maquer, et al., Bone volume fraction and fabric anisotropy are better determinants of trabecular bone stiffness than other morphological variables, J. Bone Miner. Res. 30 (6) (2015) 1000–1008.
[61] B. Voumard, et al., Influence of aging on mechanical properties of the femoral neck using an inverse method, Bone Rep. 17 (2022) 101638.
[62] V.F. Andrade, et al., Bone histomorphometry in young patients with type 2 diabetes is affected by disease control and chronic complications, J. Clin. Endocrinol. Metab. 105 (2) (2020) 506–514.
[63] J.F. Starr, et al., Robust trabecular microstructure in type 2 diabetes revealed by individual trabecula segmentation analysis of HR-pQCT images, J. Bone Miner. Res. 33 (9) (2018) 1665–1675.
[64] A.G. Nilsson, et al., Type 2 diabetes mellitus is associated with better bone microarchitecture but lower bone material strength and poorer physical function in elderly women: a population-based study, J. Bone Miner. Res. 32 (5) (2017) 1062–1071.
[65] K.M. Thrailkill, et al., Is insulin an anabolic agent in bone? Dissecting the diabetic bone for clues, Am. J. Physiol. Endocrinol. Metab. 289 (5) (2005) E735–E745.
[66] M. Unal, A. Creecy, J.S. Nyman, The role of matrix composition in the mechanical behavior of bone, Curr. Osteoporos. Rep. 16 (3) (2018) 205–215.
[67] M. Unal, Raman spectroscopic determination of bone matrix quantity and quality augments prediction of human cortical bone mechanical properties, J. Biomech. 119 (2021) 110342.
[68] B.R. McCreadie, et al., Bone tissue compositional differences in women with and without osteoporotic fracture, Bone 39 (6) (2006) 1190–1195.
[69] A.L. Boskey, et al., Examining the relationships between bone tissue composition, compositional heterogeneity, and fragility fracture: a matched case-controlled FTIRI study, J. Bone Miner. Res. 31 (5) (2016) 1070–1081.
[70] J.S. Yerramshetty, O. Akkus, The associations between mineral crystallinity and the mechanical properties of human cortical bone, Bone 42 (3) (2008) 476–482.
[71] E.M. Wölfel, et al., Human tibial cortical bone with high porosity in type 2 diabetes mellitus is accompanied by distinctive bone material properties, Bone 165 (2022) 116546.
[72] S. Lekkala, et al., Increased advanced glycation endproducts, stiffness, and hardness in iliac crest bone from postmenopausal women with type 2 diabetes mellitus on insulin, J. Bone Miner. Res. 38 (2) (2023) 261–277.
[73] S. Rokidi, et al., Bone tissue material composition is compromised in premenopausal women with type 2 diabetes, Bone 141 (2020) 115634.
[74] T. Rodic, et al., Bone quality analysis of jaw bones in individuals with type 2 diabetes mellitus—post mortem anatomical and microstructural evaluation, Clin. Oral Investig. 25 (7) (2021) 4377–4400.
[75] A. Piccoli, et al., Sclerostin regulation, microarchitecture, and advanced glycation end-products in the bone of elderly women with type 2 diabetes, J. Bone Miner. Res. 35 (12) (2020) 2415–2422.
[76] R. Dhaliwal, et al., Greater carboxy-methyl-lysine is associated with increased fracture risk in type 2 diabetes, J. Bone Miner. Res. 37 (2) (2022) 265–272.
[77] S. Arakawa, et al., Mass spectrometric quantitation of AGEs and enzymatic crosslinks in human cancellous bone, Sci. Rep. 10 (1) (2020) 18774.
[78] P.K. Zysset, et al., Elastic modulus and hardness of cortical and trabecular bone lamellae measured by nanoindentation in the human femur, J. Biomech. 32 (10) (1999) 1005–1012.
[79] E.M. Wölfel, et al., When cortical bone matrix properties are indiscernible between elderly men with and without type 2 diabetes, fracture resistance follows suit, JBMR Plus (2023) e10839.
[80] C.D.L. Thomas, et al., Femoral neck trabecular bone: loss with aging and role in preventing fracture, J. Bone Miner. Res. 24 (11) (2009) 1808–1818.
[81] R.O. Ritchie, et al., A fracture mechanics and mechanistic approach to the failure of cortical bone, Fatigue Fract. Eng. Mater. Struct. 28 (4) (2005) 345–371.
[82] N. Crabtree, et al., Intracapsular hip fracture and the region-specific loss of cortical bone: analysis by peripheral quantitative computed tomography, J. Bone Miner. Res. 16 (7) (2001) 1318–1328.
[83] P. Yang, G.-P. Brüggemann, J. Rittweger, What do we currently know from in vivo bone strain measurements in humans? J. Musculoskelet. Neuronal Interact. 11 (1) (2011) 8–20.
[84] E.F. Morgan, T.M. Keaveny, Dependence of yield strain of human trabecular bone on anatomic site, J. Biomech. 34 (5) (2001) 569–577.